Kovacs effect in a model for a fragile glass

Gerardo Aquino,[1] Luca Leuzzi,[2] and Theo M. Nieuwenhuizen[1]
[1]*Institute for Theoretical Physics, University of Amsterdam, Valckenierstraat 65, 1018 XE Amsterdam, The Netherlands*
[2]*Department of Physics, University of Rome "La Sapienza," Piazzale A. Moro 2, 00185 Roma, Italy and Institute of Complex Systems (ISC)-CNR, via dei Taurini 19, 00185 Roma, Italy*
(Received 3 December 2005; revised manuscript received 3 February 2006; published 28 March 2006)

The Kovacs protocol, based on the temperature shift experiment originally conceived by A. J. Kovacs for glassy polymers, is implemented in an exactly solvable dynamical model. This model is characterized by interacting fast and slow modes represented, respectively, by spherical spins and harmonic oscillator variables. Due to this fundamental property, the model reproduces the characteristic nonmonotonic evolution known as the "Kovacs effect," observed in polymers, spin glasses, granular materials, and molecular liquid models, when similar experimental protocols are implemented.

DOI: 10.1103/PhysRevB.73.094205 PACS number(s): 61.43.Fs, 61.20.Lc, 05.10.Ln, 05.70.Ln

I. INTRODUCTION

Systems with glassy dynamics typically exhibit nontrivial behavior when they undergo temperature shifts within the glassy phase. These systems, being in an out-of-equilibrium condition, have properties which are expected to depend on their history. This is the "memory" of glassy systems. One memory effect that shows up in a one-time observable is the so-called "Kovacs effect,"[1] which manifests itself under a specific experimental protocol. This effect has been the subject of a variety of recent investigations.[2–7] The characteristic nonmonotonic evolution of the observable under examination (the volume in the original Kovacs experiment), with the other thermodynamic variables held constant, shows clearly that a nonequilibrium state of the system cannot be fully characterized only by the (time-dependent) values of thermodynamic variables, but that further inner variables are needed to give a full description of the nonequilibrium state of the system. The memory in this case consists in these internal variables keeping track of the history of the system.

The purpose of this paper is to use a specific model for fragile glass to implement the protocol in order to get some insight into the Kovacs effect. We show that in spite of its simplicity, this model captures the phenomenology of the Kovacs effect, it makes possible to implement the Kovacs protocol not only with temperature shifts but with magnetic field shifts as well, and allows one in specific regimes to obtain analytical expressions for the evolution of the variable of interest. Furthermore, the possibility of affording a thermodynamical-like picture through the introduction of effective parameters can be investigated.

This paper is organized as follows: in Sec. II we review the experimental protocol generating the effect, in Secs. III and IV we introduce our model and use it to implement the protocol, in Sec. V we draw out of this model some analytical results, and in Sec. VI an interpretation of the effect in terms of effective parameters is illustrated with final conclusions. An appendix collects all terms and coefficients employed in the main text.

II. KOVACS PROTOCOL

The experimental protocol, as originally designed by Kovacs[1] in the 1960s, consists of three main steps.

(1) The system is equilibrated at a given high temperature T_i (see also Fig. 1).

(2) At time $t=0$ the system is quenched to a lower temperature T_l, close to or below the glass transition temperature, and it is allowed to evolve a period t_a. One then follows the evolution of the proper thermodynamic variable [in the original Kovacs experiment this was the volume $V(t)$ of a sample of polyvinyl acetate; in our model it will be the "magnetization" $m_1(t)$].

(3) After the time t_a, the volume, or other corresponding observable, has reached a value equal, by definition of t_a, to the equilibrium value corresponding to an intermediate temperature T_f ($T_l<T_f<T_i$)—i.e., such that $V_{T_l}(t_a)\equiv V_{T_f}^{eq}$. At this time, the bath temperature is switched to T_f.

The pressure (or corresponding variable) is kept constant throughout the whole experiment.

Naively one would expect the observable under consideration, after the third step, to remain constant, since it already has (at time $t=t_a^+$) its equilibrium value. But the system has not equilibrated yet and so the observable goes through a

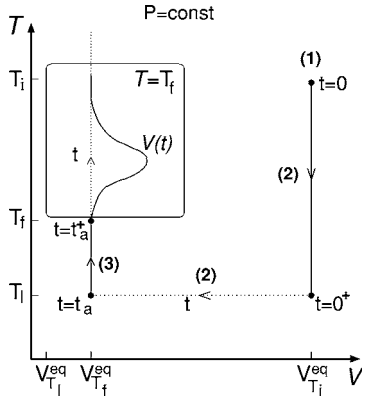

FIG. 1. *Kovacs protocol*. Starting from an equilibrium condition at $T=T_i$ [step (1)] at time $t=0$, the system is quenched to $T=T_l$ and allowed to evolve [step (2)]. In step (3) the temperature is switched to T_f. This is done at the time t_a for which $V_{T_l}(t_a)\equiv V_{T_f}^{eq}$. In the frame, the typical evolution of the volume $V(t)$ at $T=T_f$, after the final temperature switch, is illustrated.

nonmonotonic evolution before relaxing back to its equilibrium value, showing a characteristic hump whose maximum increases with the magnitude of the final jump of temperature $T_f - T_l$ and occurs at a time which decreases with increasing $T_f - T_l$.

We want to implement this protocol on a model for both strong and fragile glass first introduced in Ref. 8: the harmonic-oscillator–spherical-spin (HOSS) model. This model is based on interacting fast and slow modes; this property turns out to be necessary for the memory effect, the object of this paper, to occur.

III. HARMONIC-OSCILLATOR–SPHERICAL-SPIN MODEL

The HOSS model contains a set of N spins S_i locally coupled to a set of N harmonic oscillator x_i according to the following Hamiltonian:

$$\mathcal{H} = \sum_{i=1}^{N} \left(\frac{K}{2} x_i^2 - H x_i - J x_i S_i - L S_i \right). \tag{1}$$

The spins have no fixed length but satisfy the spherical constraint $\Sigma_{i=1}^{N} S_i^2 = N$. The spin variables are assumed to relax on a much shorter time scale than the harmonic oscillator variables, so the oscillator variables are the slow modes and on their dynamical evolution the fast spin modes act just as noise. This model is an extreme simplification of a system of particles which interact spatially via a potential and have an internal degree of freedom (rotational) with a dynamics faster than the motion of the particle itself. The potential is harmonic, and each particle interacts independently with the medium, encoded in the constant K. The inner degree of freedom (S_i) interacts only with the position of the particle (x_i), and the only global interaction is given by the spherical constraint. Due to the time scale separation, one can integrate out the spin variables to obtain the following effective Hamiltonian for the oscillators (for details see Ref. 8, explicit expressions of undefined terms appearing in all equations hereafter are reported in the Appendix),

$$\frac{\mathcal{H}_{eff}(\{x_i\})}{N} = \frac{K}{2} m_2 - H m_1 - w_T(m_1, m_2) + \frac{T}{2} \ln\left(\frac{w_T(m_1, m_2) + T/2}{T/2} \right), \tag{2}$$

which depends on the temperature and on the first and second moments of the oscillator variables: namely,

$$m_1 = \frac{1}{N} \sum_{i=1}^{N} x_i, \quad m_2 = \frac{1}{N} \sum_{i=1}^{N} x_i^2. \tag{3}$$

These variables encode the dynamics of the system which is analytically implemented through a Monte Carlo parallel update of the oscillator variables:

$$x_i \to x_i + r_i / \sqrt{N}. \tag{4}$$

The variables r_i are normally distributed with zero mean value and variance σ^2. The update is accepted according to the Metropolis acceptance rule applied to the variation $\Delta\epsilon$ of the energy of the oscillator variables, which is determined by $\mathcal{H}_{eff}$ and, in the limit of large N, is given by

$$\frac{\Delta\epsilon}{N} = \frac{K_T(m_1, m_2)}{2} \Delta m_2 - H_T(m_1, m_2) \Delta m_1. \tag{5}$$

This simple model turns out to have a slow dynamics and can be solved analytically. Following Ref. 8 one can derive the dynamical equations for m_1 and m_2:

$$\dot{m}_1 = \left[\frac{H_T(m_1, m_2)}{K_T(m_1, m_2)} - m_1 \right] f_T(m_1, m_2),$$

$$\dot{m}_2 = \frac{2}{K_T(m_1, m_2)} [I_T(m_1, m_2) + H_T(m_1, m_2) \dot{m}_1]. \tag{6}$$

The stationary solutions of these equations coincide with the saddle point of the partition function of the whole system at equilibrium at temperature T and are given by

$$\bar{m}_1 = \frac{H_T(\bar{m}_1, \bar{m}_2)}{K_T(\bar{m}_1, \bar{m}_2)} = \frac{\bar{H}_T}{\bar{K}_T},$$

$$\bar{m}_2 - \bar{m}_1^2 = \frac{T}{K_T(\bar{m}_1, \bar{m}_2)} = \frac{T}{\bar{K}_T}, \tag{7}$$

with barred variables from now on indicating their equilibrium values.

Strong and fragile glasses with the HOSS model

In spite of its simplicity, the HOSS model allows us to describe both strong and fragile glasses, characterized, respectively, by an Arrhenius or a Vogel-Fulcher law in the relaxation time. The following constraint on the configurations space is applied:

$$m_2 - m_1^2 - m_0 \geqslant 0. \tag{8}$$

When $m_0 = 0$ there exists a single global minimum in the configurations space of the oscillators which is reached at $T = 0$ and is given by

$$x_i = \frac{H + J}{L} \quad \forall\, i; \tag{9}$$

therefore, the role of the constraint with $m_0 > 0$ is to avoid the existence of a "crystalline state" and to introduce a finite transition temperature. In other words, while in the case $m_0 = 0$ there is only one ordered configuration of the oscillators fulfilling the constraint (with the equality), when $m_0 > 0$ there are many different configurations with this property. This resembles the situation where there are many metastable states which tend to trap the system. The closer the temperature gets to the transition value T_k, the longer the system is trapped in a metastable minimum. The transition temperature is directly determined by the value of the constraint parameter m_0. This constraint applied to the harmonic oscillator variables is therefore a way to reproduce the behavior of good glass formers, for which there are noncrystalline packing modes with intrinsically low energy.

The stationary solutions for the dynamics with this constraint are given by

$$\bar{m}_1 = \frac{H_T(\bar{m}_1,\bar{m}_2)}{K_T(\bar{m}_1,\bar{m}_2)} = \frac{\bar{H}_T}{\bar{K}_T},$$

$$\bar{m}_2 - \bar{m}_1^2 = \begin{cases} \dfrac{T}{K_T(\bar{m}_1,\bar{m}_2)} = \dfrac{T}{\bar{K}_T}, & T > T_k, \\ m_0, & T \leqslant T_k, \end{cases} \tag{10}$$

where T_k is determined by the further condition

$$T_k = m_0 K_{T_k}(\bar{m}_1^{T_k},\bar{m}_2^{T_k}) = m_0 \bar{K}_{T_k}. \tag{11}$$

This is the temperature above which Eq. (8) is always satisfied and the dynamics is not affected by the constraint. At $T=T_k$ the equality in (8) holds at equilibrium. Below T_k there will be $\{x_i\}$ configurations violating the constraint and therefore forbidden to the dynamic evolution. For $T \leqslant T_k$ the system can eventually reach only configurations fulfilling the equality in (8); when this happens it gets trapped forever in such a configuration. This is equivalent to having a "Kauzmann-like" transition, occurring at $T=T_k$ with vanishing configuration entropy, meaning the system gets stuck forever in one single configuration fulfilling the constraint (see also Ref. 9). When there is no constraint—i.e., when $m_0=0$—then $T_k=0$. If the Monte Carlo updates are done with Gaussian variables with constant variance σ^2, this model is characterized by an Arrhenius relaxation law

$$\tau_{eq} \sim e^{A_s/T} \tag{12}$$

in so resembling the relaxation properties of strong glasses.

The HOSS model with constraint strictly positive ($m_0 > 0$) can easily be extended to describe fragile glasses by further introducing in the variance of the Monte Carlo update the following dependence on the dynamics:

$$\sigma^2 = 8(m_2 - m_1^2)(m_2 - m_1^2 - m_0)^{-\gamma}. \tag{13}$$

In this case the relaxation time turns out to follow the generalized Vogel-Fulcher law

$$\tau_{eq} \sim e^{A_k^{\gamma}/(T-T_k)^{\gamma}}. \tag{14}$$

The parameter γ is introduced to make the best Vogel-Fulcher-type fit for the relaxation time in experiments, making this model valid for a wide range of fragile glasses. When the temperature approaches the value T_k defined by Eq. (11), from above, the system relaxes towards configurations close to the ones fulfilling the lowest bound of the constraint. The variance σ^2 then tends to diverge, the updates become large and so unfavorable, meaning that almost every update of the oscillator variables is refused. This imposes dynamically the fulfillment of the constraint and determines the diverging relaxation time following the generalized Vogel-Fulcher law of Eq. (14).

IV. KOVACS EFFECT IN THE HOSS MODEL

We implement the Kovacs protocol in the model above introduced for a fragile glass. The system is prepared at a temperature T_i and quenched to a region of temperature close to the T_k—i.e., $T_l \gtrsim T_k$. Solving numerically Eqs. (6) we determine the evolution of the system in both steps (2) and (3) of the protocol. In step (2) the time t_a at which $m_1^{T_l}(t_a) = \bar{m}_1^{T_f}$ is calculated so that

$$m_1^{T_f}(t_a^+) = \bar{m}_1^{T_f}, \quad m_2^{T_f}(t_a^+) = m_2^{T_l}(t_a). \tag{15}$$

The evolution of the fractional "magnetization"

$$\delta m_1(t) = \frac{m_1(t) - \bar{m}_1^{T_f}}{\bar{m}_1^{T_f}} \tag{16}$$

after step (3) ($t > t_a$) for different values of T_l is reported in Figs. 2 and 3, respectively, for $\gamma=1$ and $\gamma=2$.

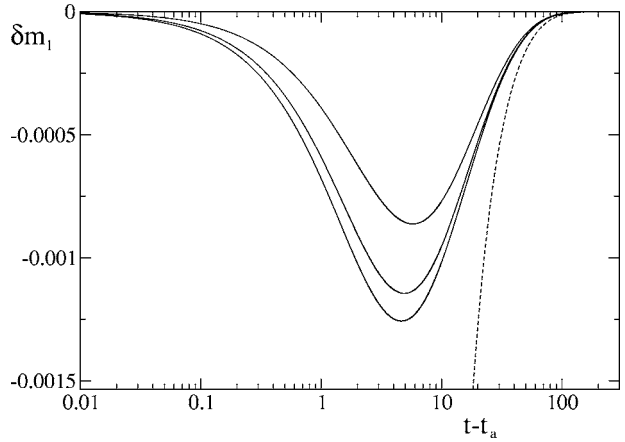

FIG. 2. *Kovacs effect in a fragile glass with* $\gamma=1$. The Kovacs protocol is implemented with a quench from temperature $T_i=10$ to T_l and final jump (at $t=t_a^+$) to the intermediate temperature $T_f=4.3$. The curves, starting from the lowest, refer to $T_l=4.005, 4.05, 4.15$; the dashed line refers to condition $T_l=T_f$ (simple aging with no final temperature shift).

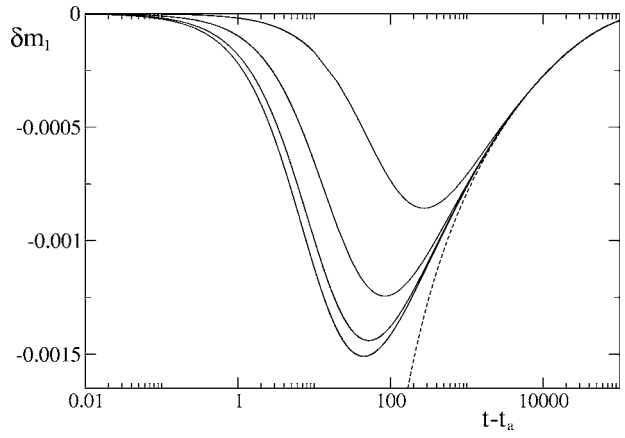

FIG. 3. *Kovacs effect in a fragile glass with* $\gamma=2$. The Kovacs protocol implemented with a quench from temperature $T_i=10$ to T_l and final jump (at $t=t_a^+$) to the intermediate temperature $T_f=4.3$. The curves, starting from the lowest, refer to $T_l=4.005$, $4.05, 4.15, 4.25$; the dashed line refers to condition $T_l=T_f$ (simple aging with no final temperature shift).

The magnetic field H is kept constant at the value $H=0.1$. In all the implementations of the protocol we use the values $J=K=1$, $L=0.1$, and $m_0=5$ for the other parameters of the model. This choice for the parameters and the value $H=0.1$ for the magnetic field fixes [through Eqs. (10) and (11)] the Kauzmann temperature at the value $T_k=4.002\,48$. Since the equilibrium value of m_1 decreases with increasing temperature (as opposed to what happens, for instance, with the volume), we observe a reversed "Kovacs hump." The curves keep the same properties typical of the Kovacs effect; the minima occur at a time which decreases and have a depth that increases with increasing magnitude of the final switch of temperature. As expected, since increasing γ corresponds to further slowing the dynamics, the effect shows upon a longer time scale in the case of $\gamma=2$ as compared to $\gamma=1$.

Actually, since in the last step of the protocol $m_1(t=t_a)=\bar{m}_1^{T_f}$ and $f_{T_f}(m_1,m_2)$ is always positive, from the first of Eqs. (6), one soon realizes that the hump for this model can be either positive or negative, depending on the sign of the term:

$$\frac{H_{T_f}(\bar{m}_1^{T_f},m_2)}{K_{T_f}(\bar{m}_1^{T_f},m_2)}-\bar{m}_1^{T_f} \tag{17}$$

at $t=t_a^+$. This term is zero when $m_1=\bar{m}_1^{T_f}$, $m_2=\bar{m}_2^{T_f}$, so one would expect $m_2(t=t_a^+)=\bar{m}_2^{T_f}$ to be the border value determining the positivity or negativity of the hump. Since $H_{T_f}(\bar{m}_1^{T_f},m_2)$ decreases with increasing m_2 while $K_{T_f}(\bar{m}_1^{T_f},m_2)$ increases, it follows that the condition for a positive hump is

$$m_2(t=t_a^+)<\bar{m}_2^{T_f}. \tag{18}$$

For shifts of temperature in a wide range close to the transition temperature T_k, where the dynamics is slower and the effect is expected to show up significantly on a long time scale, the condition $m_2(t=t_a)>\bar{m}_2^{T_f}$ is always fulfilled and therefore a negative hump is expected.

Kovacs protocol at constant temperature with magnetic field shifts

Interchanging the roles of T and H, the Kovacs protocol can be implemented at constant temperature by changing the magnetic field H instead. From Eqs. (10) and (11) one can see that the value of the transition temperature T_k depends on H as well. Different values of H determine different values of T_k. Therefore the protocol must be implemented in the following way. The temperature is kept fixed at T_i. At this temperature there is a "Kauzmann" transition for a specific value of the field $H=H_k$. The temperature T_k decreases with decreasing H. So if we work at $T=T_i$ with magnetic fields $H<H_k$, we are sure to implement every step of the protocol keeping the system always above the "Kauzmann" transition corresponding to the value of H applied. We start with the system equilibrated at $T=T_i$ and $H=H_i\ll H_k$, and at time $t=0$ we shift instantaneously the field to a larger value H_l, such that $H_i<H_l\lesssim H_k$. Then we let the system age for a time t_a such that $m_1^{H_l}(t_a)=\bar{m}_1^{H_f}$. At this time the field is shifted to H_f (with $H_f<H_l<H_k$). The subsequent evolution of the fraction magnetization $\delta m_1(t)$ is shown in Fig. 4. Again the curves show all the typical properties of the Kovacs hump, with a very slow relaxation back to equilibrium due to the choice of a value of H_f very close to H_k.

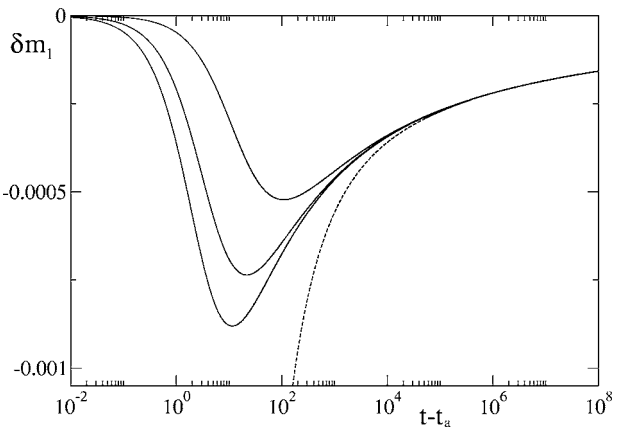

FIG. 4. *Kovacs protocol with magnetic field shifts* ($\gamma=1$). The Kovacs protocol is implemented at constant temperature $T_i=4.2$ with a sequence of magnetic field shifts. $H_k=2.24787$ is the value of the field such that $T_k=T_i=4.2$. Starting from $H_i=0.1$ [step (1)], the field is switched to H_l and the system is let to evolve a time t_a [step (2)]. At $t=t_a$—i.e., when $m_1^{H_l}(t_a)=\bar{m}_1^{H_f}$—the field is switched to $H_f=2.17$ [step (3)]. The curves, starting from the lowest, refer to $H_l=2.22, 2.20, 2.18$; the dashed line refers to the condition $H_l=H_f$.

V. ANALYTICAL SOLUTION IN THE LONG-TIME REGIME

In the previous section we have shown, through a numerical solution of the dynamics, that the HOSS model reproduces the phenomenology of the Kovacs effect, showing the same qualitative properties of the Kovacs hump as obtained in experiments (see, for example, Refs. 1 and 11), in other models with facilitated or kinetically constrained dynamics,[3,7] in models for molecular liquids,[6] and other different models.[2,4,5]

In this section we show that, by carefully choosing the working conditions in which the protocol is implemented, our model provides with an analytical solution for the evolution of the variable of interest.

A. Auxiliary variables

In order to ease calculations, as done in Refs. 8 and 9 it is convenient to introduce the following variables:

$$\mu_1=\frac{H_T(m_1,m_2)}{K_T(m_1,m_2)}-m_1,\quad \mu_2=m_2-m_1^2-m_0, \tag{19}$$

for which the dynamical equations read

$$\begin{aligned}\dot{\mu}_1&=-Q_T(m_1,m_2)I_T(m_1,m_2)\\&\quad-[1+DQ_T(m_1,m_2)]\mu_1 f_T(m_1,m_2),\\ \dot{\mu}_2&=\frac{2I_T(m_1,m_2)}{K_T(m_1,m_2)}+2\mu_1^2 f_T(m_1,m_2).\end{aligned} \tag{20}$$

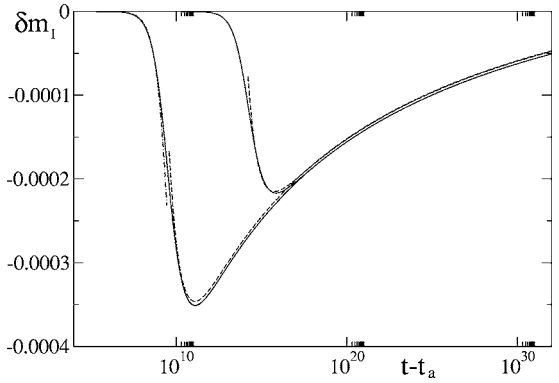

FIG. 5. Numerical solution (solid lines) of the Kovacs curves compared to the approximate analytical solution of Eq. (23) at short-intermediate (dot-dashed line) and intermediate-long $t-t_a$ (dashed line). The protocol is applied between $T_i=10$ and $T_f=4.018$. The curves starting from the lowest refer to $T_l=4.005, 4.008$ ($H=0.1$, $T_k=4.00248$).

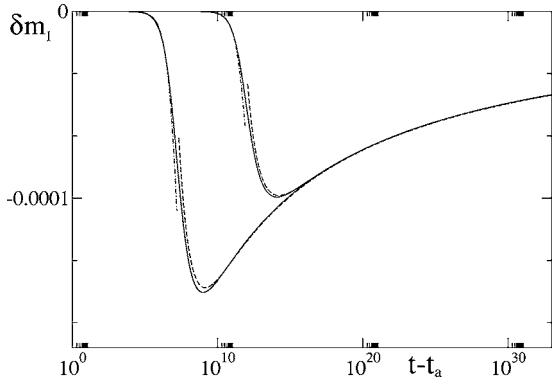

FIG. 6. Numerical solution (solid lines) of the Kovacs curves compared to the approximate analytical solution of Eq. (23) at short-intermediate (dot-dashed line) and intermediate-long $t-t_a$ (dashed line). The protocol is applied at constant temperature $T_i=4.2$ with magnetic field shifts between $H_i=0.1$ and $H_f=2.2435$. The curves starting from the lowest refer to $H_l=2.2440, 2.2438$ ($H_k=2.24787$).

We will choose to implement steps (2) and (3) of the protocol in a range of temperature very close to the Kauzmann temperature T_k. As exhaustively shown in Refs. 8 and 10 in the long time regime the variable $\mu_2(t)$ decays logarithmically to its equilibrium value which is small for $T \sim T_k$. So, if t_a is very large, the value of the variable $\mu_2(t)$, which is continuous at the jump, will be small enough to fulfill the condition for which the following equation is shown to be valid:[8]

$$\frac{d\mu_1}{d(\delta\mu_2)} = A_T(m_1,m_2)\frac{(\bar{\mu}_2+\delta\mu_2)^{-\gamma}}{\delta\mu_2}\mu_1 - \frac{JQ_T(m_1,m_2)T}{2(m_0+\bar{\mu}_2)}, \tag{21}$$

where now the variable $\delta\mu_2(t)=\mu_2(t)-\bar{\mu}_2$ is used and barred variables always refer to equilibrium condition. Of course choosing T_l close to T_k and waiting a long time t_a so that the system approaches equilibrium allows only small temperature shifts for the final step of the protocol, meaning that also T_f will be close to T_k. All the coefficients which appear in Eq. (21) (see the Appendix for the complete expressions) in the regime chosen can be assumed constant and equal to their equilibrium values with a very good approximation. The equation can then be easily integrated to give

$$\mu_1(\delta\mu_2) = \exp\left[-\bar{A}_T\frac{{}_2F_1(\gamma,\gamma,\gamma+1,-\bar{\mu}_2/\delta\mu_2)}{\gamma(\delta\mu_2)^\gamma}\right]\left(\mu_1^+\bar{B}_T^\gamma - \bar{C}_T\int_{\delta\mu_2^+}^{\delta\mu_2} dz\,\exp\left[\bar{A}_T\frac{{}_2F_1(\gamma,\gamma,\gamma+1,-\bar{\mu}_2/z)}{\gamma z^\gamma}\right]\right), \tag{22}$$

where the superscript + indicates $t=t_a^+$ and ${}_2F_1$ the hypergeometric function. This expression simplifies in cases $\gamma=1,3/2,2$. All these solutions and relative coefficients are reported in the Appendix; here, we limit ourselves to the case $\gamma=1$ which corresponds to the ordinary Vogel-Fulcher relaxation law. In this case the solution is

$$\mu_1(t) = \left(\frac{\delta\mu_2(t)}{\delta\mu_2(t)+\bar{\mu}_2}\right)^{\bar{A}_T/\bar{\mu}_2}\left[\mu_1^+\left(\frac{\delta\mu_2^+ + \bar{\mu}_2}{\delta\mu_2^+}\right)^{\bar{A}_T/\bar{\mu}_2} - \bar{C}_T\int_{\delta\mu_2^+}^{\delta\mu_2(t)} dz\left(\frac{z}{z+\bar{\mu}_2}\right)^{-\bar{A}_T/\bar{\mu}_2}\right], \tag{23}$$

where

$$\int_a^b dz\left(\frac{z}{z+\eta}\right)^\alpha = \left.\frac{{}_2F_1\left(1+\alpha,\alpha,2+\alpha,\frac{-x}{\eta}\right)x^{\alpha+1}}{\eta^\alpha(1+\alpha)}\right|_{x=a}^{x=b}.$$

One can then expand the variable of interest $m_1(t)$ in terms of μ_1 and $\delta\mu_2$ and obtain the following expression for the Kovacs curves:

$$\delta m_1(t) = A^1_{T_f}(\bar{m}_1^{T_f},\bar{m}_2^{T_f})[\mu_1(t)-\mu_1^+] + A^2_{T_f}(\bar{m}_1^{T_f},\bar{m}_2^{T_f})[\delta\mu_2(t)-\delta\mu_2^+], \tag{24}$$

where the coefficients are approximately constant in the regime chosen and can be evaluated at equilibrium.

B. Short and intermediate $t-t_a$

For small $t-t_a$, a linear approximation for the variable $\delta\mu_2$, with slope given by the second equation of the set (20) evaluated at $t=t_a^+$, turns out to be very good. Inserting this expression into Eq. (23) to get $\mu_1(t)$ and then into Eq. (24) a good approximation of the first part of the hump for small and intermediate $t-t_a$ is obtained, as shown in Figs. 5 and 6, respectively, in the case of temperature shifts and magnetic field shifts.

C. Intermediate and long $t-t_a$

When $t-t_a$ is very large, we can use Eq. (23) and the preasymptotic approximation for $\mu_2(t)$ (see Ref. 8):

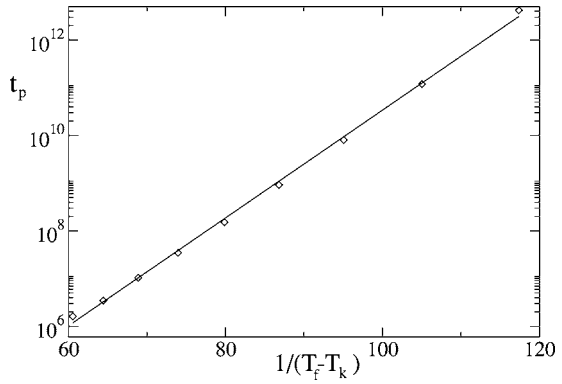

FIG. 7. Numerical calculation (diamonds) of the Kovacs peak times; the solid line is a fit with expression (27) keeping free parameters. The protocol is applied between $T_i=10$ and $T_l=4.005$. T_f is varied between 4.011 and 4.019. The parameters which give optimal fit are $t_0=0.175$ and $A_p=0.26$.

$$\mu_2(t) = \left(\ln(t/t_0) + \frac{1}{2} \ln[\ln(t/t_0)] \right)^{-1/\gamma}. \tag{25}$$

Inserting this expression into Eq. (23) to get $\mu_1(t)$ and then into Eq. (24), a good approximation for the hump and tail of the Kovacs curves is obtained. In Figs. 5 and 6 we show the agreement between the analytical expression so obtained and the numerical solution.

D. Temperature dependence of the Kovacs peak times

The analytical results obtained above in the long-time regime can be exploited to get more insight into the Kovacs effect. In Ref. 7 a direct link between the occurence time of the Kovacs peak and the relaxation properties of the glass was found numerically in a facilitated spin model; in the HOSS model, we are in a position to assess such a link also by direct analytical calculation. We can calculate the occurrence time t_p of the peak (a dip in our case) by noticing that $\dot{m}_1(t)$ is zero when $\mu_1(t)=0$ [see Eq. (6)] and so, for the case $\gamma=1$, by finding the zeros of Eq. (23). In this case it is natural to implement the protocol with a fixed T_l and changing T_f instead. Carrying out the calculation one finds

$$\mu_2^{peak} = \mu_2^+ - O(\bar{\mu}_2^2). \tag{26}$$

Using Eq. (25) and considering that in the regime chosen $\mu_2^+ \propto \bar{\mu}_2 \propto T_f - T_k$ one finally finds

$$t_p \simeq t_0 \exp\left(\frac{A_p}{T_f - T_k} \right), \quad A_p = \frac{\bar{\mu}_2}{\mu_2^+}. \tag{27}$$

We check numerically this prediction and, as shown in Fig. 7, very good agreement is displayed. The parameters of the fit coincide within the error with the theoretical value of t_0 (see the Appendix) and with A_p. The peak time, therefore, scales in the same way as the relaxation time at that temperature. This confirms, as remarked in Ref. 7, that the Kovacs protocol is sensitive to the (fragile, in this case) nature of the glass and may be used as an independent way to determine the equilibration time of the system.

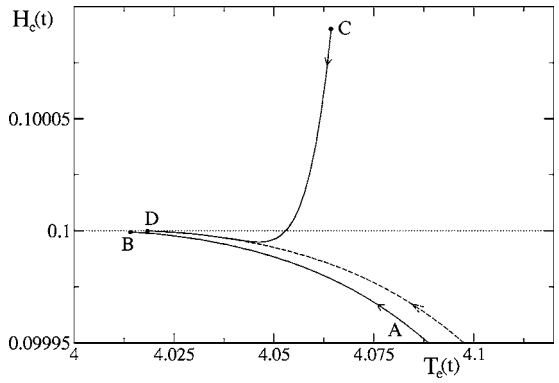

FIG. 8. *Effective field vs effective temperature in the Kovacs protocol*. The solid line *AB* refers to the last part of step (2) of the protocol—i.e., aging at $T_l=4.005$ after a quench from $T_i=10$ (we did not present the full line which starts at $T_e=9.13$ and $H_e=0.0826$, outside our picture).The solid line *CD* represents the evolution of the system in step (3) of the protocol, after an instantaneous switch of the bath temperature from $T_l=4.005$ to $T_f=4.018$ (resulting in a jump from point *B* to *C*). The nonmonotonicity of the curve *CD*—i.e., of the evolution of H_e after the jump—is the signature of the Kovacs effect. The dashed line represents simple aging at T_f after a quench from T_i. ($H=0.1$, $T_k=4.00248$)

VI. EFFECTIVE TEMPERATURE AND EFFECTIVE FIELD

The out-of-equlibrium state of the system can be expressed by a number of effective parameters which is in general equal to the number of independent observables considered. In the HOSS model, given the solution of the dynamics, a quasistatic approach can be followed to generalize the equilibrium thermodynamics (see Refs. 8 and 10) by computing the partition function of all the macroscopic equivalent states at a given time t. The measure on which this out-of-equilibrium partition function is evaluated is not the Gibbs measure. One can assume an effective temperature T_e and an effective field H_e, and substitute the equilibrium measure by $\exp(-\mathcal{H}_{\text{eff}}(\{x_i\},T,H_e)/T_e)$ and, in this way, determine the partition function and then the free energy. The values of the effective parameters at a given time t are those that minimize the free energy so calculated. In this way one then obtains

$$T_e(t) = K_T(m_1(t),m_2(t))[m_2(t) - m_1^2(t)],$$

$$H_e(t) = H - K_T(m_1(t),m_2(t))\mu_1(t). \tag{28}$$

We plot H_e as a function of T_e in a Kovacs setup in Fig. 8. We see that in step (2) of the protocol (lower solid line), equivalent to a simple aging experiment, the effective magnetic field relaxes monotonically to the value H. In step (3) (upper solid line *CD*), after the final jump of the bath temperature, represented in the figure by the jump from point *B* to point *C*, the effective magnetic field goes through a nonmonotonic evolution before relaxing to the equilibrium value H. This is when the "Kovacs" effect occurs. A conclusion that can be drawn is that a thermodynamiclike picture in terms of only the effective temperature is not possible in the Kovacs setup if not at cost of neglecting effects of the order

of magnitude of the "Kovacs effect" itself. So, while in an aging experiment in the long-time regime $H_e(t)-H$ is very small compared to $T_e(t)-T$ (so that one can consider $H_e=H$ and use only T_e as effective parameter), in the Kovacs protocol, it is in the nonmonotonic evolution of the effective field that the memory effect manifests itself. An additional effective field is then needed to recover a complete thermodynamiclike picture of the system inclusive of the Kovacs effect. The dashed line in the figure represents a simple aging experiment at $T=T_f$; in this case a thermodynamiclike picture with only an effective temperature is possible, assuming $H_e=H$. One can argue from the figure that such a picture would be possible also in step (3) of the protocol (curve *CD*) since the two curves, for T_e close enough to T_f, coincide. But this happens when the system is close to equilibrium and the signature of the memory effect, the nonmonotonic evolution, is lost. These conclusions confirm the results obtained in Ref. 6, where the impossibility of a thermodynamiclike picture with only the effective temperature was based on a potential energy landscape (PEL) analysis. The molecular liquid studied in Ref. 6, in the last step of the Kovacs protocol, explores regions of the PEL never explored in equilibrium, and so a simple mapping to an equilibrium condition at a different temperature (the effective temperature by definition) is not possible.

VII. CONCLUSION

We have shown that a simple mode with constrained dynamics like the HOSS model, is rich enough to reproduce the Kovacs memory effect, even allowing one to obtain an analytical expression for the Kovacs hump in a long-time regime. The Kovacs effect is observed in many experiments and models, showing common qualitative properties which we have found to be shared also by the model analyzed in this paper. The quantitative properties depend on the particular system or model analyzed.

As far concerns the HOSS model, it turns out that for the slow modes—i.e., the oscillator variables—fixing the overall average value, the magnetization m_1, does not prevent the existence of memory encoded in the variable m_2, which keeps track of the history of the system. The equilibrium value of m_2 increases with temperature while the equilibrium value of m_1 decreases with increasing temperature. Therefore, after the final switch of temperature, since $m_2(t_a) > \bar{m}_2^{T_f}$, the variable m_2 has a value corresponding to an equilibrium condition at a higher temperature (memory of the initial state at temperature T_i) so driving the system towards a condition corresponding to a higher temperature—i.e., smaller values of m_1—determining the hump.

It is important to stress that a fundamental ingredient in the HOSS model is the interaction between slow and fast modes. Due to this interaction, the equilibrium configurations of the oscillator variables at a given temperature are determined by both m_2 and m_1, the first and second moments of their distribution, whose dynamical evolution is interdependent. When such an interaction is turned off (by setting $J=0$) essentially only one variable is sufficient to describe both the equilibrium configurations and the dynamics of the system, and the memory effect is lost. In this respect this model constitutes an improvement to the so-called oscillator model[12] within which such a memory effect cannot be reproduced. The model provides us with an anlytical solution for the Kovacs curves in a specific regime ($T \gtrsim T_k$, long times), allowing us to get an expression for the peak times which turn out to scale in the same way as the equilibrium relaxation time of the system at that temperature. This confirms that, as found also in Ref. 7 on different models, the Kovacs protocol provides one with an independent way to assess the nature of the relaxation properties of the system. Another important conclusion, confirming previous results,[6] which can be drawn from this model is that a complete thermodyanmiclike picture inclusive of the Kovacs effect, with only an effective temperature, is not possible and that also an effective field in this case is needed. In the present model one can also study temperature cycle experiments of the type carried out in spin glasses (see Ref. 13), leaving room for further research.

ACKNOWLEDGMENTS

G.A. and L.L. gratefully acknowledge the European network DYGLAGEMEM for financial support. We thank Stefano Mossa for interesting discussion.

APPENDIX

In this appendix we report all explicit expressions for terms appearing in the text. In Eqs. (2), (5), and (6) we have

$$w_T(m_1,m_2) = \sqrt{J^2 m_2 + 2JLm_1 + L^2 + T^2/4},$$

$$K_T(m_1,m_2) = K - \frac{J^2}{w_T(m_1,m_2) + T/2},$$

$$H_T(m_1,m_2) = H + \frac{JL}{w_T(m_1,m_2) + T/2},$$

$$f_T(m_1,m_2) = \frac{\sigma^2 K_T(m_1,m_2)}{2T} \mathrm{Erfc}[\tilde{\alpha}_T(m_1,m_2)] \times \exp[\tilde{\alpha}_T^2(m_1,m_2) - \alpha_T^2(m_1,m_2)],$$

$$I_T(m_1,m_2) = \frac{\sigma^2 K_T(m_1,m_2)}{4} \mathrm{Erfc}[\alpha_T(m_1,m_2)] + \left(\frac{T}{2} - K_T(m_1,m_2)\tilde{w}_T(m_1,m_2)\right) f_T(m_1,m_2),$$

where

$$\tilde{w}_T(m_1,m_2) = m_2 - m_1^2 + \left(\frac{H_T(m_1,m_2)}{K_T(m_1,m_2)} - m_1\right)^2,$$

$$\alpha_T(m_1,m_2) = \sqrt{\frac{\sigma^2}{8\tilde{w}_T(m_1,m_2)}},$$

$$\frac{\tilde{\alpha}_T(m_1,m_2)}{\alpha_T(m_1,m_2)} = \frac{2K_T(m_1,m_2)\tilde{w}_T(m_1,m_2)}{T} - 1.$$

In Eqs. (12), (14), and (21)–(24),

$$A_s = \frac{\sigma^2 \bar{K}_T}{8}, \quad D = JH + LK = JH_T + LK_T,$$

$$Q_T(m_1,m_2) = \frac{J^2 D}{K_T^3 w_T (w_T + T/2)^2},$$

$$P_T(m_1,m_2) = \frac{J^4 (m_2 - m_1^2)}{2K_T w_T (w_T + T/2)^2},$$

$$A_k = \frac{\bar{K}_{T_k}(K - \bar{K}_{T_k})(1 + D\bar{Q}_{T_k} + \bar{P}_{T_k})}{(K - \bar{K}_{T_k})(1 + D\bar{Q}_{T_k}) - \bar{K}_{T_k}\bar{P}_{T_k}},$$

$${}_2F_1(a,b,c,z) = \frac{\Gamma(c)}{\Gamma(a)\Gamma(b)} \sum_{n=0}^{\infty} \frac{\Gamma(a+n)\Gamma(b+n)}{\Gamma(c+n)} \frac{z^n}{n!},$$

$$A_T(m_1,m_2) = \frac{[1 + Q_T(m_1,m_2)D]^2}{1 + P_T(m_1,m_2) + Q_T(m_1,m_2)D},$$

$$\bar{B}_T^{\gamma} = \exp\left[\bar{A}_T \frac{{}_2F_1(\gamma,\gamma,\gamma+1,-\bar{\mu}_2/\delta\mu_2^+)}{\gamma(\delta\mu_2^+)^{\gamma}} \right],$$

$$\bar{C}_T = \frac{JQ_{T_f}(\bar{m}_1^{T_f},\bar{m}_2^{T_f})T_f}{2(m_0 + \bar{\mu}_2)} = \frac{J\bar{Q}_{T_f}T_f}{2(m_0 + \bar{\mu}_2)},$$

$$A_T^1(m_1,m_2) = \frac{(w_T + T/2)K_T}{m_1[Jm_1 + L + (w_T + T/2)K_T]},$$

$$A_T^2(m_1,m_2) = 2m_1 A_T^1(m_1,m_2),$$

$$t_0 = \frac{\sqrt{\pi}}{8\gamma} \frac{1 + D\bar{Q}_T}{1 + D\bar{Q}_T + \bar{P}_T}.$$

Solutions of Eq. (21) *for* $\gamma = \frac{3}{2}$:

$$\mu_1(\delta\mu_2) = \left(\frac{1 - \sqrt{1 + \delta\mu_2/\bar{\mu}_2}}{1 + \sqrt{1 + \delta\mu_2/\bar{\mu}_2}} \right)^{\bar{A}_T/\bar{\mu}_2^{3/2}} e^{2\bar{A}_T/(\bar{\mu}_2\sqrt{\bar{\mu}_2 + \delta\mu_2})} \left[\mu_1^+ \bar{B}_T^{3/2} - \bar{C}_T \int_{\delta\mu_2^+}^{\delta\mu_2} dz \left(\frac{1 + \sqrt{1 + z/\bar{\mu}_2}}{1 - \sqrt{1 + z/\bar{\mu}_2}} \right)^{\bar{A}_T/\bar{\mu}_2^{3/2}} e^{-2\bar{A}_T/(\bar{\mu}_2\sqrt{\bar{\mu}_2 + z})} \right].$$

Solutions of Eq. (21) *for* $\gamma = 2$:

$$\mu_1(\delta\mu_2) = \left(\frac{\delta\mu_2}{\delta\mu_2 + \bar{\mu}_2} \right)^{\bar{A}_T/\bar{\mu}_2^2} e^{\bar{A}_T/[\mu_2^2(1 + \delta\mu_2/\bar{\mu}_2)]} \left[\mu_1^+ \bar{B}_T^2 - \bar{C}_T \int_{\delta\mu_2^+}^{\delta\mu_2} dz \left(\frac{z}{z + \bar{\mu}_2} \right)^{-\bar{A}_T/\bar{\mu}_2^2} e^{-\bar{A}_T/[\bar{\mu}_2^2(1 + z/\bar{\mu}_2)]} \right].$$

[1] A. J. Kovacs, Fortschr. Hochpolym.-Forsch. **3**, 394 (1963); A. J. Kovacs, J. J. Aklonis, J. M. Hutchinson, and A. R. Ramos, J. Polym. Sci., Polym. Chem. Ed. **17**, 1097 (1979).

[2] L. Berthier and J-P. Bouchaud, Phys. Rev. B **66**, 054404 (2002).

[3] A. Buhot, J. Phys. A **36**, 12367 (2003).

[4] E. M. Bertin, J-P. Bouchaud, J-M. Drouffe, and C. Godrèche, J. Phys. A **36**, 10701 (2003).

[5] L. F. Cugliandolo, G. Lozano, and H. Lozza, Eur. Phys. J. B **41**, 87 (2004).

[6] S. Mossa and F. Sciortino, Phys. Rev. Lett. **92**, 045504 (2004).

[7] J. J. Arenzon and M. Sellitto, Eur. Phys. J. B **42**, 543 (2004).

[8] L. Leuzzi and Th. M. Nieuwenhuizen, Phys. Rev. E **64**, 011508 (2001).

[9] Th. M. Nieuwenhuizen, cond-mat/9911052 (unpublished).

[10] Luca Leuzzi, Ph.D. thesis, Universiteit van Amsterdam, 2002.

[11] C. Josserand, A. Tkachenko, D. M. Mueth, and H. M. Jaeger, Phys. Rev. Lett. **85**, 3632 (2000).

[12] L. L. Bonilla, F. G. Padilla, and F. Ritort, Physica A **250**, 315 (1998).

[13] E. Vincent, J. Hamman, M. Ocio, J-P. Bouchaud, and L. F. Cugliandolo, in *Complex Behaviour of Glassy Systems*, Springer Verlag Lecture Notes in Physics, Vol. 492, edited by M. Rubi (Springer, Berlin, 1997), pp. 184–219.